To evaluate eqn. 4, noise current source i_i should be determined accurately. The empirical formula given in [5] was employed in this work. Applying Dragone's theory for diodes [6] to this empirical formula, the correlation between the mth and nth mixing frequencies of i_i was evaluated as

$$\overline{i_{i,m} i_{i,n}^*} = 4KTB\left[\frac{I_{ds}(t)}{V_{ds}(t)} \cdot P(t)\right]_{m-n} \quad (5)$$

where $[\ ]_{m-n}$ is $(m-n)$th Fourier coefficient. Parameter P has been extracted for various MESFETs and HEMTs and turned out to be very close to 1. In this work, P was set to 1.

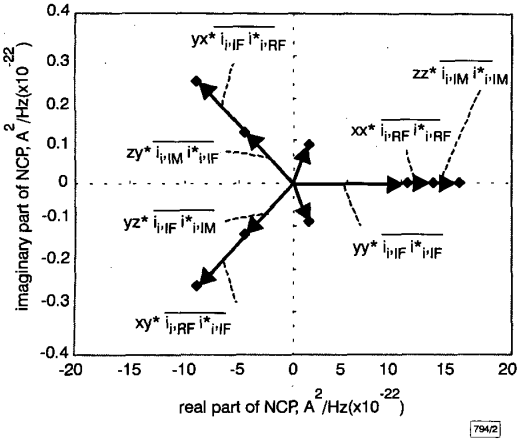

Fig. 2 *Phasor diagram of noise current power ($\overline{i_i^2}$) due to intrinsic noise source at $P_{LO} = -1$dBm*

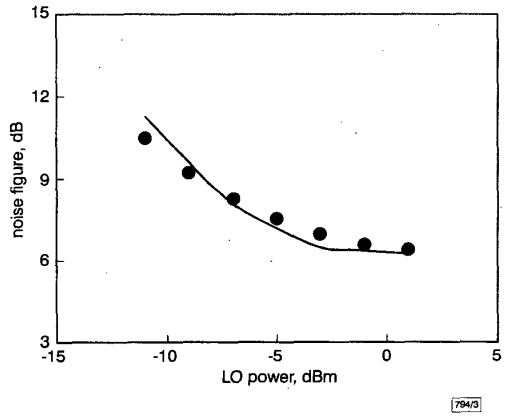

Fig. 3 *Comparison of measured and modelled noise figures in FET resistive mixers*

RF frequency 9.7GHz
LO frequency 10GHz
——— analytical expression
● measurement data

Simplification and validation: To verify the analysis method, a hybrid-type resistive mixer using 0.25μm PHEMTs was designed and fabricated to operate at 10GHz. Using a table-based nonlinear model, a single-tone harmonic balance simulation was performed to evaluate the harmonic components of G_{ds} at various LO power levels. Following the analysis presented earlier, contributions from each frequency component of the intrinsic noise (each term in eqn. 4) were evaluated and expressed in phasor form as in Fig. 2. Dominant components can, in this way, be easily found. The following observations can be made on the intrinsic noise source contribution: (i) self-terms in eqn. 4 add in-phase, (ii) correlation between IF and IM and IF and RF frequency components add out-of-phase with the self-terms, reducing the total noise level.

After identifying dominant components, a simplified analytical expression can be obtained in the following form:

$$F = 1 + \frac{1}{\mathrm{Re}[Z_s(\omega_{RF})]} \cdot \left\{ \left(2 + \frac{\overline{|L_{IF}|^2}}{\overline{|L_{RF}|^2}}\right)(R_s + R_d) + \left(2\overline{|Z_{s,RF}|^2} + \frac{\overline{|L_{IF}|^2}}{\overline{|L_{RF}|^2}}\overline{|Z_{l,IF}|^2}\right) G_{ds_0} + 2\,\mathrm{Re}[L_{RF} L_{IF}^* Z_{s,RF} Z_{l,IF}^* G_{ds_1}] \right\} \quad (6)$$

where $Z_{s,RF} = Z_s(\omega_{RF}) + R_s + R_d$ and $Z_{l,IF} = Z_l(\omega_{IF}) + R_s + R_d$. Eqn. 6 can be used as a first-order design formula for noise figures in FET resistive mixers.

The modelled noise figure data were compared with measurements in Fig. 3. Excellent agreement was found between the measured and modelled noise figure at various LO power levels.

Conclusion: An analytical analysis method for the evaluation of noise figures in FET resistive mixers has been developed. For better accuracy, an empirical noise model was employed to represent the intrinsic noise source. A phasor diagram analysis has enabled a physical understanding of the mixing mechanism to be obtained and allowed a simplified noise figure formula to be developed which can be used as a first-pass design tool.

23 April 1999
Electronics Letters Online No: 19990791
DOI: 10.1049/el:19990791

Won Ko and Youngwoo Kwon (*School of Electrical Engineering, Seoul National University, San 56-1, Shinlim-dong, Kwanak-ku, Seoul, Korea*)

References

1 MAAS, S.A.: 'A GaAs MESFET mixer with very low intermodulation', *IEEE Trans.*, 1987, **MTT-35**, pp. 425–429
2 VIRK, R.S., and MAAS, S.A.: 'Modeling MESFETs for intermodulation analysis of resistive FET mixers', *IEEE MTT-S Dig.*, 1995, **3**, pp. 1247–1250
3 PENG, S.: 'A simplified method to predict the conversion loss of FET resistive mixers', *IEEE MTT-S Dig.*, 1997, pp. 857–860
4 HELD, D.N., and KERR, A.R.: 'Conversion loss and noise of microwave and millimeter-wave mixers: Part 1 - Theory', *IEEE Trans.*, 1978, **MTT-26**, pp. 49–55
5 FOLKES, P.A.: 'Thermal noise measurements in GaAs MESFET's', *IEEE Electron Device Lett.*, 1985, **EDL-6**, pp. 620–622
6 DRAGONE, C.: 'Analysis of thermal shot noise in pumped resistive diodes', *Bell Syst. Tech. J.*, 1968, **47**, pp. 1881–1902

Efficient hybrid method for characterisation of arbitrary-shaped discontinuities in rectangular waveguide

Jongkuk Park, Heeduck Chae and Sangwook Nam

An efficient hybrid method is proposed for analysing discontinuities in a rectangular waveguide. With only a small number of meshes around discontinuities, the typical finite element method is shown to give an exact solution through several iterative updates of the boundary conditions. To demonstrate the validity of the proposed method, a simple circular aperture in a rectangular waveguide is analysed and results compared with those of another method.

Introduction: The finite element method has been used as a powerful tool for solving arbitrary-shaped discontinuities in shielded structures. However, for open region problems, it has difficulties in discretising infinite domains since the finite element meshes must be terminated far away from the obstacle so that the abrupt termination of meshes has no effect on the solution. To overcome these shortcomings, the iterative hybrid method was proposed to solve electrostatic and TM 2D scattering problems in open space, and found to give a good result in open region problems [1, 2]. In the case of applying the finite element method to waveguide problems, the fictitious plane for terminating meshes should be placed far enough from the obstacle so that higher-order modes excited by the obstacle die out before they reach the plane. This requires a large number of meshes, and the number of unknowns becomes

large. Thus, the finite element-boundary integral method [3, 4] has been used to avoid these problems, and it is shown to be more efficient [4] than the ordinary finite element method. But this method, proposed in [3, 4], has a drawback that its system matrix has lost the sparsity of an ordinary finite element matrix.

In this Letter, to solve three-dimensional waveguide discontinuities more efficiently, an iterative finite element method is proposed. This method gives an accurate result, but the meshes required by this method are terminated so close to the discontinuities that computational efforts can be greatly reduced. In addition, since sparsity in the system matrix is preserved, it does not take more time to find the inverse of the system matrix than required by an ordinary finite element method.

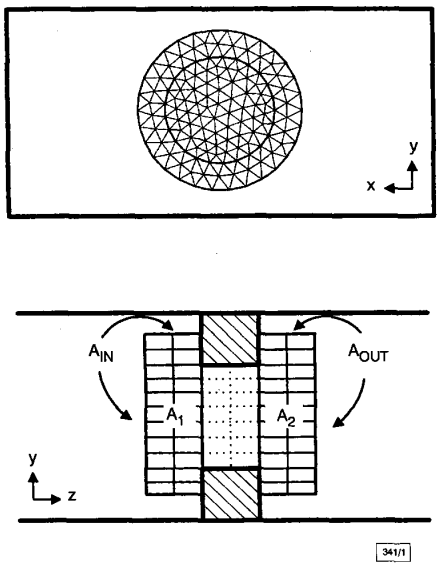

Fig. 1 *Simple circular aperture in rectangular waveguide and finite element meshes for proposed method*

Theory: As a simple example, a cross-sectional aperture in a rectangular waveguide is analysed. Since the aperture is uniform along the wave propagation axis, triangular prism elements [3] are used. Fig. 1 shows the structure and the volume to be discretised. The extended boundary layer in Fig. 1 can be reduced to only one without much loss of accuracy. In Fig. 1, A_{IN}, A_{OUT} are fictitious surfaces on which the Dirichlet boundary condition should be determined. Fig. 2 describes the whole procedure of the proposed method. First, the initial fields on A_{IN}, A_{OUT} are assumed. Since these fields would be updated later, it can be determined arbitrarily. In this Letter, the dominant TE_{10} mode is assumed to exist on A_{IN}, A_{OUT} initially. Once the boundary condition is determined in this way, the typical finite element procedure is applied. With the Dirichlet boundary condition, the function is as follows:

$$F(\vec{E}) = \frac{1}{2}\int_V \frac{1}{\mu_r}(\nabla \times \vec{E})\cdot(\nabla \times \vec{E}) - k_0^2 \varepsilon_r \vec{E}\cdot\vec{E}\, dv \quad (1)$$

With this function minimised, the field on A_1, A_2 can be determined. From the surface equivalence theorem and image theory, the imaginary magnetic current source is introduced and this source updates the field on A_{IN}, A_{OUT}. Since the fields on the boundary are total fields, the fields on the input boundary are composed of the incident field, the field reflected by the conducting plane, and the field scattered by the equivalent magnetic current source, while the fields on the output are composed of only the field scattered by the equivalent source. The incident field and the reflected field are known. The scattered fields on the boundary can be evaluated using eqn. 2:

$$\vec{E}_{scat} = 2\int_{A_i} \hat{x} M_{yi}\frac{\partial G_{Fyy}}{\partial z} - \hat{y} M_{xi}\frac{\partial G_{Fxx}}{\partial z} + \hat{z}\left(M_{xi}\frac{\partial G_{Fxx}}{\partial y} - M_{yi}\frac{\partial G_{Fyy}}{\partial x}\right) dS' \quad (2)$$

where A_i represents the surface A_1 or A_2, and M_{xi}, M_{yi} are equivalent magnetic currents on A_i. G_{Fxx}, G_{Fyy} are potential Green functions in a rectangular waveguide. Since the Green function inherently has a slow convergence property, we have accelerated the calculation of the Green function using the Poisson summation formula and the Kummer transform [5]. The numerical integration of the Green function can be regarded as the most time consuming in this method. However, it must be carried out at the first iteration, and the results can be used in the subsequent iterations. Therefore, this is not a serious problem. In this way, once the boundary condition is updated, the same procedure is repeated

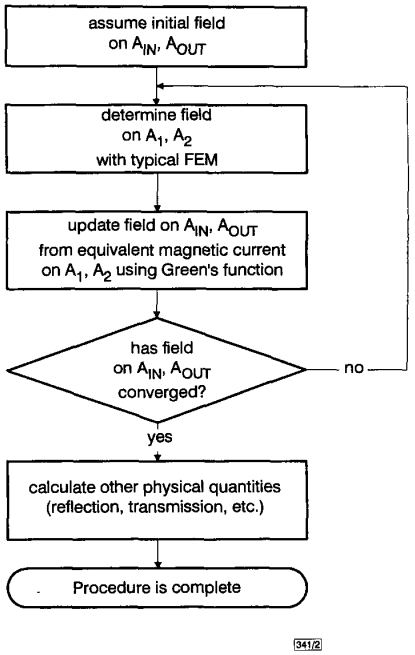

Fig. 2 *Entire procedure of iterative finite element method*

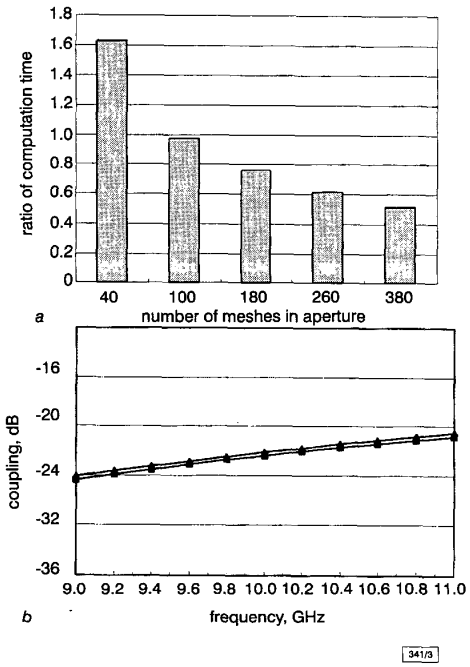

Fig. 3 *Comparison of results between this method and FEBIM [3]*

a Computation time against number of meshes in aperture
□ t_{IFEM}/t_{FEBIM}
b Transmission results obtained by using proposed method and [3]
—■— IFEM
—▲— FEBIM

until the difference between the current boundary fields and updated boundary fields at the next iteration process reduces to the prescribed error criterion. Since this iteration process is completed within only several repetitions, the proposed method is considered to give an efficient solution for waveguide discontinuities.

Numerical results: For a circular aperture with radius 0.3cm in WR-90, the performance of the proposed method is compared with that of the finite element-boundary integral method [3]. As shown in Fig. 3, the proposed method gives a result in good agreement with [3] and is more efficient in terms of computation time.

Conclusions: A novel iterative finite element method has been applied to a waveguide problem. The proposed method is shown to be not only simple to use but also very effective since it exploits a typical finite element procedure with only a small number of meshes and it requires only several periods of iterations. Therefore, this method is thought to represent an efficient tool for the analysis of various types of waveguide discontinuities.

1 June 1999
Electronics Letters Online No: 19990794
DOI: 10.1049/el:19990794

Jongkuk Park, Heeduck Chae and Sangwook Nam (*School of Electrical Engineering, Seoul National University, San 56-1, Shilim-Dong, KwanAk-Gu, Seoul, 151-742, South Korea*)

References

1 ROY, T., SARKAR, T.K., DJORDJEVIC, A.R., and SALAZAR-PALMA, M.: 'A hybrid method for terminating the finite element mesh (electrostatic case)', *Microw. Opt. Technol. Lett.*, 1995, **8**, (6), pp. 282–287
2 ROY, T., SARKAR, T.K., DJORDJEVIC, A.R., and SALAZA, M.: 'A hybrid method solution of scattering by conducting cylinders (TM case)', *IEEE Trans.*, 1996, **MTT-44**, (12), pp. 2145–2151
3 PARK, J., and NAM, S.: 'Analysis of arbitrary shaped crosssectional discontinuity in rectangular waveguides using FEM-BIM with triangular prism elements'. IEEE AP-S Int. Symp., Montreal, Canada, 1997, pp. 672–675
4 PARK, J., and NAM, S.: 'A general rigorous analysis of arbitrary-shaped multiaperture-coupled directional coupler between two dissimilar rectangular waveguides crossing with an arbitrary angle', *Microw. Opt. Technol. Lett.*, 1998, **18**, (1), pp. 43–46
5 AHN, B.C.: 'Moment method analysis of a narrow wall inclined slot on a rectangular waveguide'. Ph.D. Dissertation, University of Mississippi, Oxford 1992

Circuit implementation of K-winner machine

S. Ridella, S. Rovetta and R. Zunino

The K-winner machine (KWM) model for supervised classification enhances vector quantisation by characterising classification outcomes with confidence levels. Each data-space location is assigned a specific local bound to the error probability. Structural simplicity makes the implementation compatible with circuitry for classical VQ, and features high speed and efficiency.

KWM model: A prototype-based schema spans the data space by a set of reference positions ('prototypes', 'codewords'). The maximum similarity drives the categorisation process, which classifies each sample with the class of the best-matching prototype. Thus vector quantiSation (VQ) involves a winner-takes-all (WTA) schema, and partitions the data space into as many Voronoi subregions as the number of prototypes. The samples lying in a region are classified according to the related prototype. WTA-based categorisation is not usually characterised by a confidence measure: as far as classification is concerned, all points within a region are equivalent and with an equal confidence value.

The K-winner machine (KWM) overcomes such a drawback by taking into account, for each test sample, a larger set of prototypes including K elements ($K \geq 1$). Similarly to WTA, the KWM uses the 'winning' prototype to set classification; however, it also seeks the largest number K of best-matching prototypes that agree with the winner. The level of agreement depends on the test location, hence each data point yields a specific value of K. The basic assumption is that a point with a large K value denotes high confidence in the associate classification. The KWM embeds classical WTA in the minimal case $K = 1$: when even the second best-guess disagrees with the winning candidate, confidence reaches its minimum. A WTA classifier and a KWM involve the same representation structure, i.e. a set of class-calibrated prototypes positioned in the data space by some VQ algorithm. Thus KWM training does not differ from any conventional VQ-classifier setup. Instead, the KWM run-time operation for classifying a sample $\mathbf{x}$ can be outlined as follows:

(i) compute the distance d_n between $\mathbf{x}$ and each prototype $\mathbf{w}_j$, $j = 1, ..., N_h$
(ii) sort the list of prototypes in order of increasing d_n
(iii) work out the largest K value such that $\text{Class}(\mathbf{w}_k) = \text{Class}(\mathbf{w}_1)$ $\forall k = 1, ..., K$
(iv) *a* classify $\mathbf{x}$ according to the winning prototype, $\text{Cl}(\mathbf{w}_1)$ ($\equiv$ WTA classification).
b prompt K as the confidence level for the present classification outcome.

Measuring the agreement among prototypes (step (iii)) helps predict the generalisation performance: it can be proved [1] that the Vapnik-Chervonenkis dimension [2] of a K-winner machine can be computed exactly as

$$d_{VC} = \lfloor N_h / K \rfloor \tag{1}$$

Therefore, by using eqn. 1 and basic results from generalisation theory [1], we set a bound on the KWM classifier's error probability π, given by

$$\pi = \nu + \sqrt{\frac{1}{N_p}\left[d_{VC}\left(1 + \ln\frac{2N_p}{d_{VC}}\right) - \ln\frac{\eta}{4}\right]} \tag{2}$$

where ν is the classification error for a training set including N_p samples, and η (typ. = 0.05) is a confidence parameter.

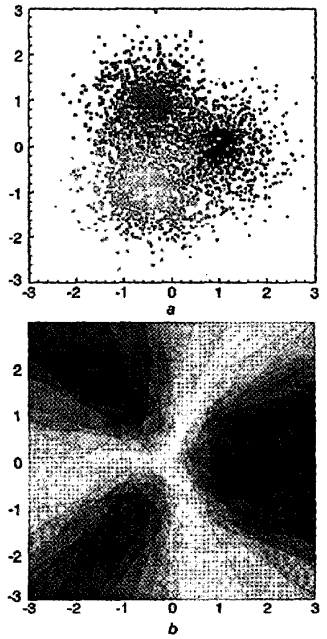

Fig. 1 *KWM results on Gaussian-mixture testbed*
a Training data (three classes)
b Confidence map; darker areas denote higher K and higher confidence; bright regions (low K) span class boundaries

In summary, for each test location in the data space, we first compute the local K value, then by using [1, 2] we determine a bounded estimate of the expected error probability. The opportunity to predict the generalisation ability analytically and at the local level represents a crucial advantage of the KWM model. A KWM differs from a voting schema substantially, as prototypes